Three-dimensional Structure of the Acetylcholine Receptor by Cryoelectron Microscopy and Helical Image Reconstruction

Chikashi Toyoshima and Nigel Unwin

Medical Research Council Laboratory of Molecular Biology, Cambridge CB2 2QH, England

Abstract. Long tubular vesicles have been grown from isolated *Torpedo* postsynaptic membranes, in which the receptors are arranged helically on the vesicle surface. The structures of these tubes have been analyzed by cryoelectron microscopy of specimens embedded in thin films of ice, combined with helical image reconstruction. Complete data sets from tubes belonging to several helical families have been obtained to a resolution of 17 Å in all directions. Confirming a preliminary study (Toyoshima, C., and N. Unwin. 1988. *Nature (Lond.).* 336:247–250), the central ion channel has an almost constant diameter throughout the molecule except for the portion extending through the hydrophobic part of the lipid bilayer, where the pore is too small to be resolved. However, the density on the pseudo fivefold axis running through the pore is consistently highest in the cytoplasmic half of the bilayer, suggesting the gate is located in that region. The path followed by each subunit has been identified throughout the length of the receptor. The two α subunits follow equivalent paths. All subunits have similar features which change in character at the same level relative to the membrane.

The nicotinic acetylcholine receptor is the most well studied member of a superfamily of neurotransmitter-gated ion channels, which includes the GABA$_A$ and glycine receptors (for recent reviews, see references 5, 7, 24, 33). It consists of five subunits arranged with pseudo fivefold symmetry around a pore (2, 3), which forms a cation-selective pathway across the membrane (20). Two of these subunits (α) have the same amino acid sequence, and the other three (β, γ, and δ) are homologous (∼ 40% identity to the α subunits) (31). In addition, all five subunits are glycosylated, leading to estimated molecular masses of 52 (α), 56 (β), 61 (γ), and 64 kD (δ) (5, 33).

Most recent experimental evidence, combined with analyses of the amino acid sequence, suggest a topography for the receptor in which each subunit has four transmembrane α-helices (Ml–M4) and both the NH$_2$- and COOH-terminals are on the synaptic side of the membrane (reviewed in reference 7). From photo-cross-linking experiments with noncompetitive blockers, which are thought to enter into the pore and physically block the channel, it is presumed that at least a part of M2 lines the pore (15, 16, 21, 35). Site-directed mutagenesis of critical amino acids has shown further that residues flanking (22) and within (6, 28) M2 directly affect the ion transport behavior of the channel.

Information on the three-dimensional structure of this molecule has come largely from electron crystallographic studies of postsynaptic membranes isolated from *Torpedo* electroplaques (2, 3, 25, 27, 37, 39). The receptor is an elongated molecule that protrudes from the membrane by ∼60 Å into the synaptic cleft and by ∼ 20 Å into the cytoplasm of the cell. The structure inside and near the membrane is of particular interest in relation to the function of the channel. We showed in a previous paper (37) that there are abrupt changes in structure at the level of phospholipid head groups: the pore becomes very narrow where it passes through the hydrophobic part of the bilayer, and is unresolvable at 17 Å resolution, whereas it has a much wider diameter (20–25 Å) throughout the rest of its length.

Here we extend earlier work on the structure of the receptor, using vesicles of postsynaptic membranes isolated from *Torpedo marmorata* electroplaques. We induce these native membranes to form long, narrow tubes in which the receptors are organized in crystalline arrays (2). The cylindrical symmetry of the tubes is preserved by rapid freezing of specimens suspended over holes in carbon support films, and three-dimensional maps are derived from three separate classes of tube by helical image reconstruction. The structure determined in this way is free from the limitations associated with tilting methods, where it is impossible to collect a complete range of views. By virtue of these techniques, the data are complete at 17 Å resolution. The maps we describe represent density of protein and lipid (rather than stain excluding density) averaged over >9,000 molecules. The whole structure, including the interior of the membrane and the inside of the tube, is clearly visualized.

C. Toyoshima's present address is Department of Biological Sciences, Tokyo Institute of Technology, Ookayama, Meguro-ku, Tokyo 152 and Bioelectronic Materials, Frontier Research Program, RIKEN, Wako, Saitama 351-01, Japan.

© The Rockefeller University Press, 0021-9525/90/12/2623/13 $2.00
The Journal of Cell Biology, Volume 111 (No. 6, Pt. 1), Dec. 1990 2623–2635

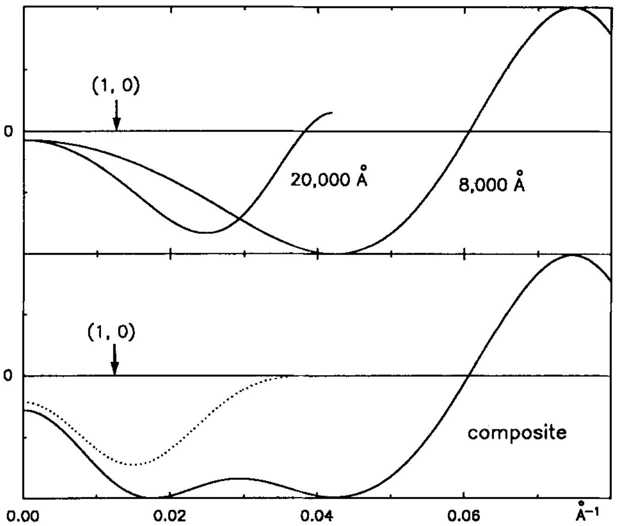

Figure 1. Contrast transfer functions for images of the acetylcholine receptor tubes in ice (38). The curves are calculated for a first image at 8,000 Å underfocus and for a second image at 20,000 Å underfocus. The upper panel shows the curve for each image and the lower panel shows the curve for the composite. To obtain the composite, the second image was first low-pass filtered to put more weight on lower spatial frequency terms (*dotted line*), and then the Fourier transforms of the images were added up to their respective zeros in the contrast transfer function. This procedure resulted in a similar weighting for all the Fourier terms to a resolution of 17 Å. The spatial frequency corresponding to the (1, 0) reflection from the flattened tubes (2) is indicated.

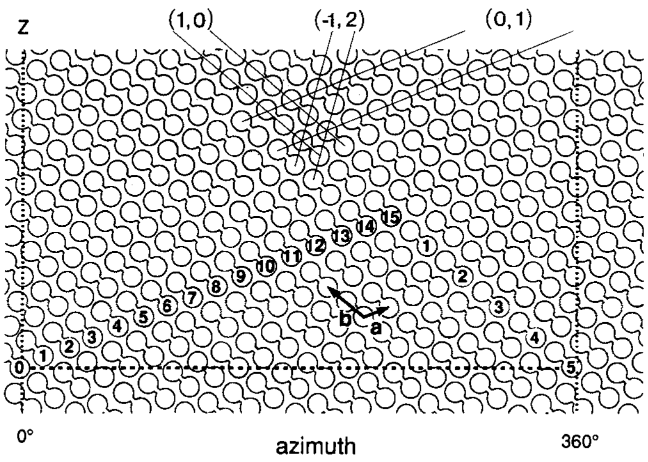

Figure 2. Diagram of the surface lattice of an acetylcholine receptor tube. The surface lattice consists of a regular array of receptor dimers (indicated by the linked circles) arranged on a cylindrical surface, and the diagram is made by opening such a cylinder and viewing it from outside. The horizontal axis shows azimuthal angle and the vertical axis is parallel to the tube axis. A line on the surface lattice corresponds to a helix. The surface lattice can be characterized by numbers (start numbers) of two principal lines (helices) required to fill 360° of azimuth; in this case a 15 start left-handed helix and a 5 start right-handed helix, denoted by (1, 0) and (0, 1), respectively, are the principal helices; they give rise to the (1, 0; −15) and (0, 1; 5) layer-lines, according to the (*h*, *k*; *n*) indexing scheme used here (see Materials and Methods). This surface lattice is referred to as of the (−15, 5) class. Several lines (helices) and the unit cell vectors (*a* and *b*) are indicated.

Materials and Methods

Electron Microscopy

Tubular vesicles of acetylcholine receptors crystallized in the native lipids were prepared from electric organs from *Torpedo marmorata* as described (27). 5 μl of the specimen solution were deposited on the carbon side or both sides of holey carbon grids (36). Excess solution was blotted with dried filter paper and the grids were frozen rapidly by plunging them into liquid ethane slush cooled to ∼−160°C by liquid nitrogen. They were stored in liquid nitrogen until use. Specimens were examined at low temperature (−168°C) using a prototype cryo-holder (Mark II; Gatan, Inc., Warrendale, PA) and Philips EM400T or 420T electron microscopes operated at 120 kV. Both microscopes were fitted with a low dose kit and an auxiliary twin-bladed anticontaminator.

Two low dose pictures (∼10 electrons/Å^2 each) were taken of each field, the first one at ∼8,000 Å and the second one at ∼20,000 Å underfocus, using a nominal magnification of 36,000×. Two images were necessary because the contrast of different periodicities in the images is not uniformly transferred from the object and thus a single picture cannot cover completely the required range with a good signal-to-noise ratio (38). To achieve approximately uniform contrast transfer, the second image was low-pass filtered and the Fourier terms of this image were added to those of the first image. Fig. 1 shows curves of transferred contrast, calculated for individual images and for the composite image. The dotted line in the lower panel shows the curve for the low-pass filtered second image. The contrast transferred for the composite image at the spacing corresponding to the lowest order diffraction peaks is ∼80% of the maximum, assuming 7% amplitude contrast (38).

This method involving the summation of two images at two different levels of underfocus does not, however, give accurate weights for the Fourier terms at very low resolution (>100 Å spacing). Such terms are found on the equator (central horizontal line in the diffraction pattern) and arise from the mean radial variations in density. Although extensive measurements have yet to be made, preliminary measurements show that even at very low resolution the amplitude contrast is still ∼7%. The effect of the contrast transfer function on the equatorial data was therefore corrected using the theoretical contrast transfer function for 7% amplitude contrast. This correction, when applied to either of the two differently underfocused images, gave essentially the same result for the mean radial density distribution.

Indexing of Layer-lines

The diffraction from a helical particle can be considered as an extension of that from a two-dimensional crystal and related to the surface lattice. Fig. 2 shows a surface lattice relevant to the receptor tube. In this figure, lines following a certain direction represent a set of helices and may be characterized by crystallographic (*h*, *k*) indices. A particularly important parameter for defining a surface lattice is the number of lines (helices) required to make up the circumference. Due to the cylindrical nature, these numbers (start numbers) must be integral. In Fig. 2, the start numbers for the two principal sets of lines corresponding to the unit cell vectors, namely (1, 0) and (0, 1), are 15 and 5, respectively. Taking the direction (handedness) into account, this surface lattice is referred to as of the (−15, 5) class.

Each set of lines on the surface lattice will give rise to a layer-line conventionally characterized by (*n*, *l*) indices, where *n* refers to the start number of the contributing helix and *l* (layer-line number) shows the axial height of the layer-line (26). From the close correspondence between the surface lattice and the (*n*, *l*) plot (26), there is a simple linear relationship between (*h*, *k*) and (*n*, *l*) indices. For example, if *n* and *l* for the (1, 0) and (0,1) lines are given as n_{10} and l_{10}, etc., *n* and *l* for (*h'*, *k'*) layer-line will be $n' = h' \cdot n_{10} + k' \cdot n_{01}$ and $l' = h' \cdot l_{10} + k' \cdot l_{01}$; thus the start number for, say, the (0, 5) line must be a multiple of 5. By use of this relationship and the rule ($2\pi rR \sim= 1.1 \cdot |n| + 0.9$) relating the distance from the axis of density in real space (*r*) to radius of the amplitude maximum along the layer-line (*R*) (26), it was usually possible to assign *n* to each layer-line unequivocally. The handedness of one principal helix has been determined in earlier experiments (39). Determination of the layer-line number (*l*) depends on the repeat distance of the helix, which was established by a correlation method (see below). Assignment of (*h*, *k*) indices to each layer-line was based on the indexing system used with flattened tubes (2). Table I lists some of these indices and radii for the (−15, 5) class of tube.

Table I. Helical Parameters for the Particles Belonging to the (-15, 5) Class

h	k*	n	l‡	R_{peak}§	r_{peak}‖
				Å^{-1}	Å
−1	2	25	8	0.0132	338
−2	4	50	16	0.0245	338
2	−2	−40	14	0.0204	337
1	0	−15	22	0.0088	342
0	2	10	30	0.0085	288
−1	4	35	38	0.0178	339
2	0	30	44	0.0156	340
1	2	−5	52	0.0032	340
0	3	15	45	0.0091	305
0	4	20	60	0.0109	334
0	5	25	75	0.0142	306
0	6	30	90	0.0173	308

* (h, k) indices are according to Brisson and Unwin (1984).

‡ Layer-line number (l) and the start number of the contributing helix (n) are according to the selection rule of $l = 3n + 67m$ ($n = 5n'$) and repeat distance of 2,196 Å.

§ Position of the first intensity peak along the layer-lines of the averaged dataset.

‖ Radii of corresponding peaks in density in real space; determined using g_{nl}, obtained by Fourier-Bessel synthesis of the averaged layer-line data (11).

Analysis of Images

Images of narrow receptor tubes in which the straight part extended >4,000 Å were examined by optical diffraction. Those weakly and strongly underfocused pairs of images that gave symmetrical diffraction patterns and no indication of drift were selected for further analysis. Digitization was carried out with flatbed microdensitometers manufactured by Perkin-Elmer Corp. (Norwalk, CT) or Joyce, Loebl and Co., Ltd. (Gateshead, England) (extensively modified in-house) using a scanning interval of 15 μm (corresponding to 4.3 Å on the specimen).

The digitized images were first interpolated in real space so that an exact multiple of the repeat distance was included in the 512 × 1,024 Fourier transform. This made all the layer-lines in the Fourier transform fall on the sampling raster and minimized the interpolation involved. To determine the repeat distance and the rotation angle with respect to the sampling raster, different portions of the image that were between 1,200 and 6,000 Å from a reference area were searched for maximum correlation. Typically, two or three parts of the same tube, each ~4,000 Å long (one to four repeats), were Fourier transformed and averaged in Fourier space.

The position of the helix axis was refined by minimizing the sum of amplitude-weighted phase residuals (Table II) between corresponding peaks on either side of the meridian (the axis lying parallel to the axis of the tube). Since no significant differences in the level and positions of amplitude maxima were observed between the two sides, they were simply averaged to improve the signal-to-noise ratio. Twofold symmetry, demonstrated previously for the flattened vesicles (2), was well preserved (Table II) and was used for aligning different images. Datasets from the different stretches of the same tube were brought to a common twofold origin. Then, all the datapoints on every possible layer-line up to the first zeros of the contrast transfer functions were averaged.

Different tubes belonging to the same helical family, which had different layer-line numbers (l) but the same start numbers (n) and (h, k) indices, had their layer-line numbers reassigned for averaging. This could be done since the amplitude and phase profiles of layer-lines having the same n and (h, k) indices but different l were indistinguishable at 17 Å resolution. The alignment of individual images was performed against the averaged dataset after twofold enforcement. Those portions of the averaged layer-lines that showed good consistency with two-fold symmetry were incorporated in a Fourier-Bessel inversion. Three-dimensional density maps were calculated by Fourier synthesis (11, 26).

The structure of the receptor determined by these procedures is essentially equivalent to that determined by the procedures used to analyze the flattened tubes (3), as was confirmed by comparing projection maps (Fig. 3). In the projection normal to the helix axis (Fig. 3 *a*), curvature of the cylindrical tube restricts comparison to the molecule located at the center of the figure. However, many features of the receptor are essentially the same as in the projection normal to the plane of the flattened tube (Fig. 3 *b*). Small differences between the two types of projections would be expected because of the slightly different superposition of densities from neighboring molecules. The good overall correlation indicates that a high signal-to-noise ratio is achieved by either approach.

Results

Images of the Receptor Tubes

The images selected for helical analysis were of straight and narrow (<800 Å diam) tubular vesicles suspended in thin amorphous ice over holes in the carbon support film. The diameter of the tubes was variable, with a lower limit of ~650 Å; however, only restricted discrete values were apparently allowed for the diameter of narrowest tubes and, as

Table II. Phase Residuals and Fitting Parameters for the Particles Belonging to the (-15, 5) Class

Image numbers*	Number of molecules averaged	Intraparticle phase residuals‡ (degrees)	Two-fold phase residuals§ (degrees)	R-factor‖	Radial scaling factor	Interparticle phase residuals¶ (degrees)
305/306	2,320	11.8(42)/ 11.7(34)	15.7 (42)	0.159	1.005	15.30
617/618	1,855	13.3(38)/ 10.0(31)	19.7 (41)	0.249	1.004	18.94
3,391/3,392	3,903	12.3(38)/ 10.6(36)	11.1 (43)	0.132	0.986	13.06
4,489/4,490	1,341	11.1(31)/ 9.9(31)	12.8 (37)	0.261	1.005	21.92

* A pair of images (the first image at ~8,000 Å and the second image at ~20,000 Å underfocus) constitute one set.

‡ Intraparticle phase residual Q as defined by DeRosier and Moore (1970); upper row for the first image; lower row for the second. The numbers in the parentheses indicate the numbers of data points used.

§ Amplitude weighted phase residuals for twofold symmetry (difference from either 0 or 180°, whichever closer) of the composite dataset (i.e., the second image was low-pass filtered and added at an appropriate weight to the first image); the summation was taken over all the points with amplitude higher than 3% of the highest off-equatorial amplitude. The equator was omitted from the calculation. The numbers in the parentheses indicate the numbers of layer-lines included in the calculation.

‖ Crystallographic R-factor defined as sum of (| averaged amplitude − individual amplitude |)/(sum of averaged amplitude); the summation was taken as in the third footnote.

¶ Interparticle phase residuals (P (40) or R_{min} (1)) against the final twofold forced averaged dataset.

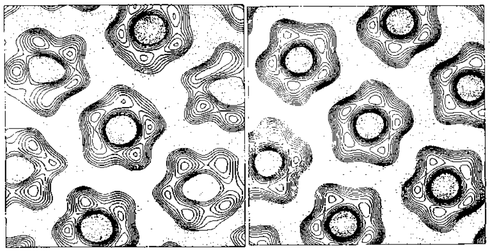

Figure 3. Comparison of projections normal to the membrane from (*a*) cylindrical tubes of the (−15, 5) class, and (*b*) flattened tubes. The projection from cylindrical tubes was obtained by projecting three-dimensional densities calculated from an averaged dataset; only the sections between r = 230 and 360 Å were used to obviate excessive overlapping of densities from the neighbouring molecules. The projection from flattened tubes (*b*) was made by Fourier synthesis of diffraction data from six sides. Due to the curvature of the cylindrical tube, only the molecule located at the center can be compared. Images were taken under identical conditions (36,000× nominal magnification; ∼8,000 Å underfocus). No corrections were made for the contrast transfer function.

shown later, only one type of helical lattice was consistent with each of them.

Fig. 4 shows micrographs of three classes of tubes that were analyzed. They are designated (−15, 5), (−17, 5), and (−16, 6) to indicate the type of helical surface lattice (see Materials and Methods). Features are somewhat different from the wider flattened tubes analyzed previously (3), because the cylindrical symmetry is now well preserved. In particular, the gentler curvature at the periphery of these tubes has made the ladder-like stack of short bars running along their edges less conspicuous. The tube "wall" also appears thicker than in the case of the flattened tubes and four parallel lines can be seen to run along both edges (most obvious when viewing along the tube at glancing angle).

Diffraction Patterns

Images of narrow tubes such as those shown in Fig. 4 gave diffraction patterns consisting of a series of horizontal lines (layer-lines) extending to better than 1/20 $Å^{-1}$ (Fig. 5). The layer-lines are symmetrical about the vertical axis (meridian), showing that the two sides of the tubes have a similar density distribution. Although the diffraction from the cylindrical tubes is different from that of the flattened tubes, the patterns made by the higher intensity peaks on the layer-lines (cylindrical tubes) and by the diffraction peaks (flattened tubes) are similar. Thus, if (h, k) indices are assigned to the layer-lines, the diffraction patterns from both types of specimen can be treated in a consistent way. Furthermore, although the distances from the meridian and from the equator are different from tube to tube, the (h, k) indices are the same, independent of the diameter of the tube and the repeat distance.

In helical diffraction patterns, the distances of peaks from the meridian characterize the class of tube and reflect its three-dimensional organization: the distances (R_{peak} in Table I) are related to the start numbers of helices (n) and the radii in real space where the variation in density is maximum (r_{peak} in Table I). For the tubes belonging to the same class, the start numbers (n) are the same, but the layer-line numbers (l) may well be different, since they depend on the repeat distance, which is highly variable. Considering the merits of different indices, we use h, k, and n indices, rather than conventional n and l indices, and the notation (h, k; n) to designate a particular layer-line.

Table I shows that the largest variations in density are found near the periphery of the tube (radius of ∼340 Å) for most of the helices. However, the radii of the highest densities (r_{peak}) contributing to the (0, k; 5k) layer-lines, notably to the (0, 2; 10) layer-line, are smaller. Consistent with this difference, the intensity peak on the (0, 2; 10) layer-line is shifted away from the line drawn from the origin to the peak on the (0, 6; 30) layer-line. This means that the densities contributing to the (0, 2; 10) layer-line are at a different radius from those contributing to the other layer-lines. This is consistent with the fact that the (0, 2; 10) layer-line is strongly affected by alkaline treatment of the tubes, which alters the density at the cytoplasmic extremity of the receptor (37).

Averaging of Different Images

Averaging of different tubes was made difficult by the fact that they all had different unit cell parameters and repeat distances. Nevertheless, most of narrowest tubes belonged to one of the three classes shown in Fig. 4, and there was the possibility of averaging tubes belonging to the same class if the variations in unit cell parameters were sufficiently small. These variations were examined by drawing unit cells at the outermost radius of the tube, where the variations were most pronounced. Fig. 6 shows unit cells of the tubes belonging to the (−15, 5) class. The variations were greatest along the b cell direction (up to ±3.0 Å); the variations along the a cell direction were smaller (<±1 Å). This difference is also typical of the other classes of tubes. Thus, the distortion introduced by the averaging, in all classes, would be <4 Å, which is much smaller than the resolution achieved (17 Å) and therefore can be neglected.

The averaging of different tubes in a given helical class provides an opportunity to evaluate specimen preservation and hence quality of the data. Results from tubes of the (−15, 5) class are presented in most detail, since the number of tubes that were averaged is the greatest (four tubes and >9,000 molecules averaged). Moreover, tubes in this class have the smallest diameter, making them the least prone to flattening. Table II lists the values obtained for several fitting parameters (radial scaling factors, interparticle phase residuals, and R-factors). The radial scaling factor is influenced by variations in magnification and deformation of the specimen, and the differences in this parameter were very small, indicating that flattening is not a significant factor. Small numbers for the interparticle phase residuals and R-factors justify the averaging of different particles and confirm the good preservation of the specimens.

The amplitude and phase variations along three layer-lines from the averaged dataset of the (−15, 5) class of tubes are shown in Fig. 7. The (1, 0; −15) layer-line is typical of a strong layer-line; it has 20 peaks along the layer-line up to 1/20 $Å^{-1}$, the phases of which are very close to 0 or 180°, indicating good twofold symmetry. The (−2, 4; 50) layer-line has a large number, 50, for n; the phase deviation from

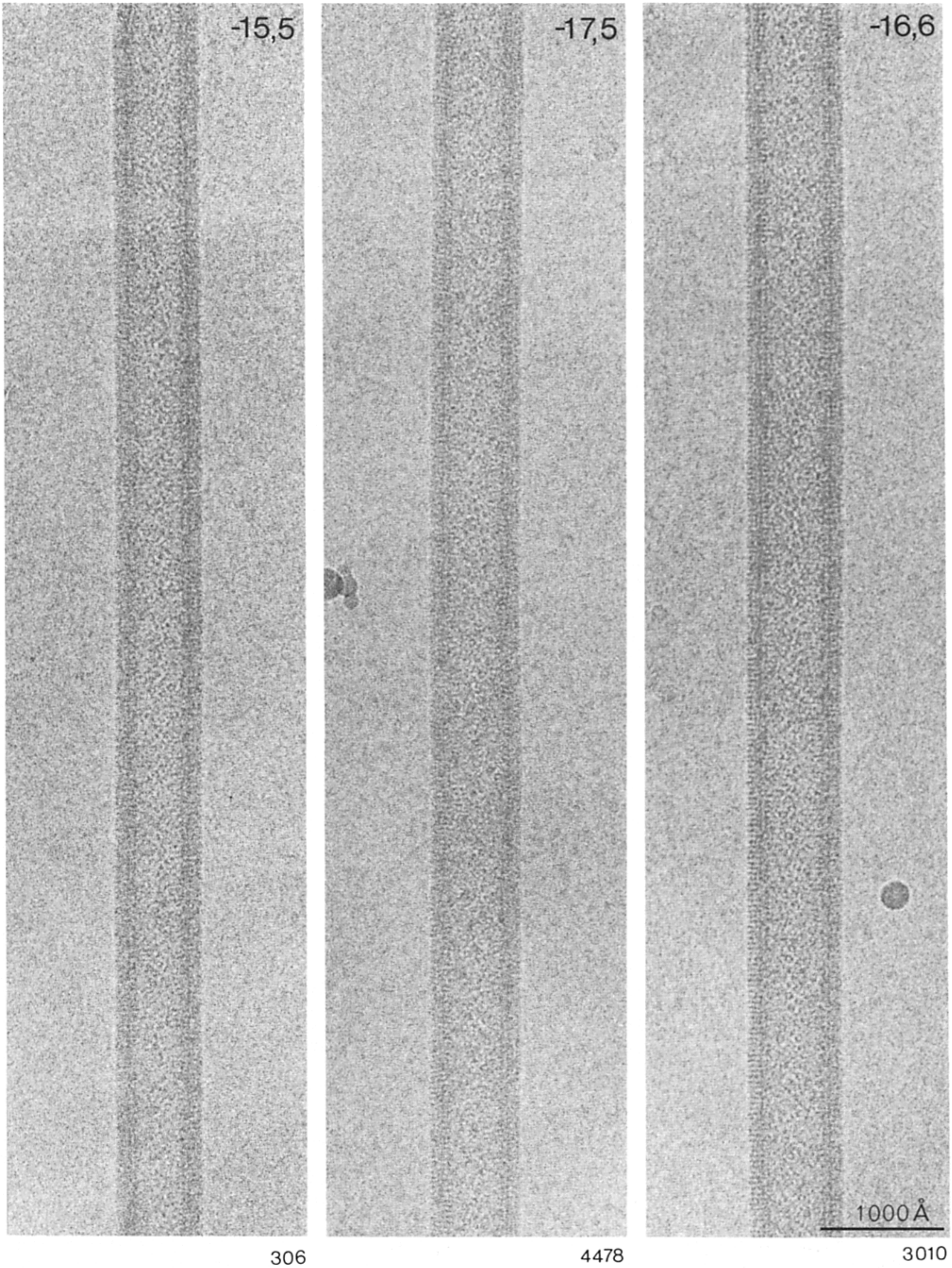

Figure 4. Electron micrographs of the acetylcholine receptor tubes in ice. The receptor tubes were rapidly frozen and embedded in ice over holes in the carbon support film. The specimens were not stained, and hence the images represent the true distribution of densities in the specimens. The three tubes shown have different diameters and belong to different helical families. The two indices at the right hand side corner indicate the start numbers of two principal helices (see Materials and Methods and Fig. 2). Note that four parallel lines run along the edges of each tube (most easily seen by looking along their axes at glancing angle). These lines correspond to densities at the cytoplasmic end of the receptor (I), the inner (II) and the outer (III) leaflets of the lipid bilayer, and the synaptic part of the receptor (IV) (see also Fig. 8). The tubes belonging to the (−15, 5) class are ∼700 Å in diameter.

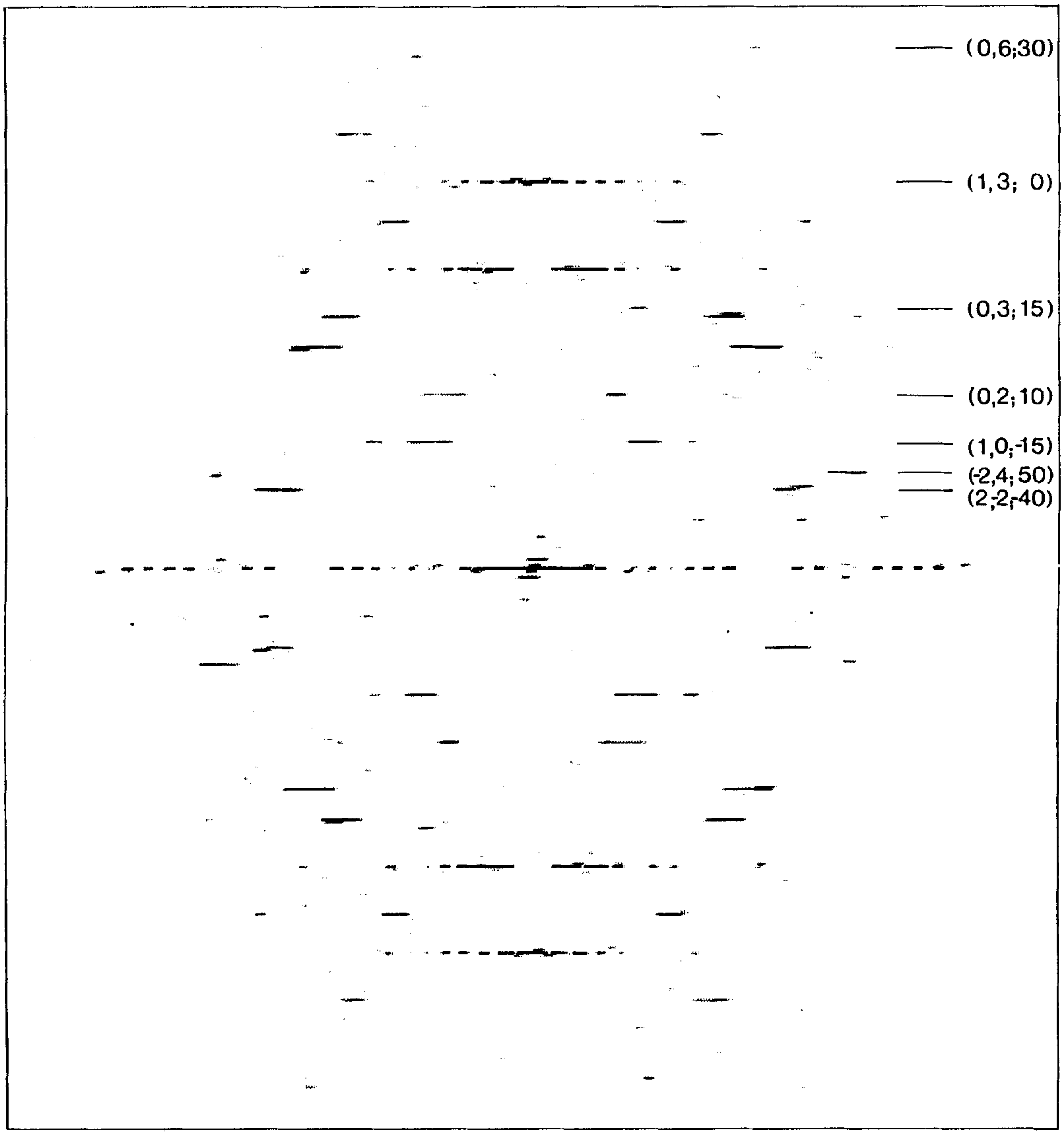

Figure 5. Diffraction pattern from a receptor tube taken at ~8,000 Å underfocus. The (*h*, *k*; *n*) indices for major layer-lines are shown, where *h* and *k* refer to the indices of corresponding surface lattice lines (helices) and *n* refers to the start number of contributing helices (see Fig. 2). Positive and negative *n*s correspond to right-handed and left-handed helices, respectively. This diffraction pattern is from a tube belonging to the (−15, 5) class. The meridional (1, 3; 0) layer-line has a spacing of ~1/30 $Å^{-1}$. Note that the first peak on the (0, 2; 10) layer-line does not fall on the line drawn from the origin to the peak on the (0, 6; 30) layer-line, showing densities at considerably different radii are contributing to these two layer-lines.

either 0 or 180° is not as good as for the (1, 0; −15) layer-line, possibly due to slight misalignment of the helix axis relative to the sampling raster. The (1, 5; 10) layer-line is at higher resolution (spacing along the meridian: ~1/20 $Å^{-1}$); although the amplitude is much weaker than for the other two layer-lines, the phases at amplitude maxima are again close to 0 or 180°. The amplitude weighted phase residual for two-fold symmetry of the averaged dataset (see legend to Table II) was 5.7°.

The equatorial layer-line has an important role in helical reconstruction because it gives information about the mean density distribution in the radial direction. Fig. 8 shows mean radial density distributions (g_{00}) obtained by Fourier-Bessel synthesis of equatorial data from three tubes in the (−15, 5) class, together with the averaged distribution. The curves are similar and consist of four peaks. These four peaks are related to the four parallel lines running along both edges of the tubes (Fig. 4) and correspond to the density at the cytoplasmic end of the receptor (I), the inner (II) and outer (III) leaflets of the bilayer, and the synaptic portion of the receptor (IV), respec-

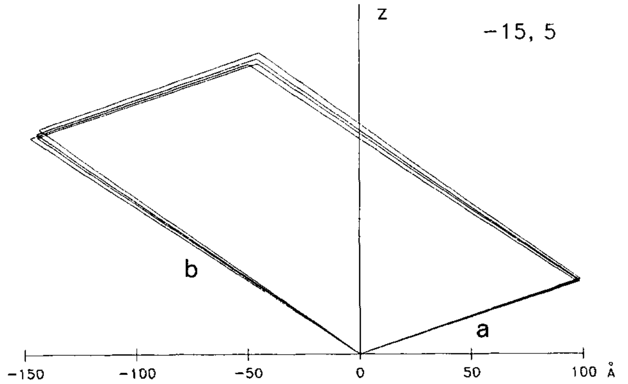

Figure 6. Unit cells for four tubes belonging to (−15, 5) class, at a radius of 350 Å. The mean unit cell parameters (a = 103.7 Å; b = 174.7 Å; included angle 127.3°) were determined after scaling corrections. Note that the variation in length of the *b* vector is larger than that of the *a* vector. In either direction, the difference is less than ± 3 Å.

tively (37). The distances between these peaks were nearly constant irrespective of the diameter of the tube and the curves for different classes of tubes were directly superimposable (data not shown).

Three-dimensional Maps of the Receptor Tube

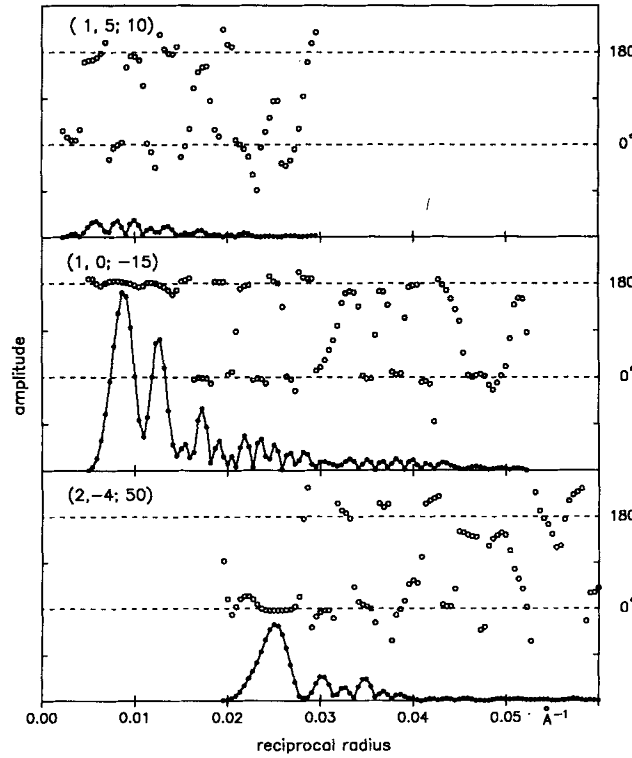

Figure 7. Amplitude and phase variations along three layer-lines from the (−15, 5) class of tube. About 9,400 molecules from four tubes have contributed to these averaged layer-lines. Indices (*h*, *k*; *n*) are shown. Note that the phases are close to either 0 or 180°, particularly where the amplitudes are strong, indicative of good twofold symmetry.

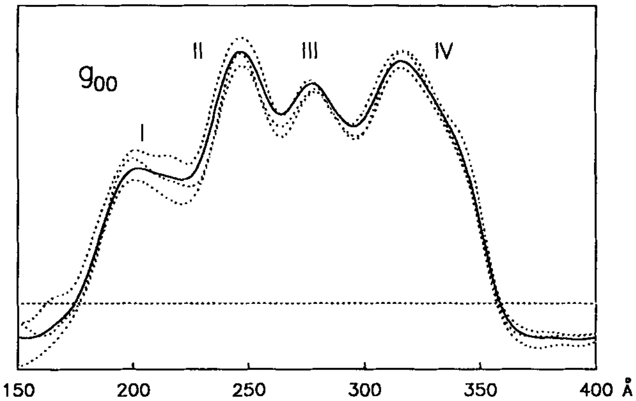

Figure 8. Mean radial density distribution (g_{00}) from three individual tubes belonging to the (−15, 5) class (*broken lines*) and their average (*solid line*). The curves were obtained by Fourier-Bessel synthesis of Fourier terms along the equatorial layer-line, after correcting for the effects of the contrast transfer function. The four peaks marked correspond to four lines seen along the edge of the tubes (Fig. 4) and refer respectively to densities at the cytoplasmic end of the receptor (I), the inner (II) and the outer (III) leaflets of the lipid bilayer, and the synaptic part of the receptor (IV) (see also Fig. 8). Note that the three individual g_{00}s are very similar except for rather large differences at peak I, which has been attributed to a receptor associated protein (37).

A three-dimensional structure with helical symmetry can be considered as made up from a series of coaxial cylinders of density. Fig. 9 represents such a cylinder calculated for a radius (r = 300 Å), just outside the membrane. At this radius, ribbons of paired receptors are formed by associations between subunits of neighboring molecules that were determined previously (27) to be δ and α. The ribbons follow the *a* vector of the unit cell (Fig. 9). Below we describe the three-dimensional structure of the tube in terms of horizontal cross-sections normal to the axis of this cylinder (Fig. 10) and in terms of vertical sections parallel to the cylinder axis (Fig. 11).

Horizontal Cross Sections. Fig. 10 shows cross sections calculated from three different helical families of tubes at a level corresponding to the horizontal line in Fig. 9. The inner (Fig. 10, *I*) and outer (*O*) leaflets of the lipid bilayer are resolved, and the receptor (*R*) is seen to protrude by ~60 Å from the membrane surface on the synaptic side but only ~20 Å on the cytoplasmic side. A density, presumed to represent the 43-kD protein (37), is located centrally over the receptor at the cytoplasmic end.

These cross sections cut individual receptors in different places, but have been chosen to include a cut through the center of a molecule as well (Fig. 9). The section from the tube in Fig. 10 *a* has fivefold rotational symmetry and so the pattern repeats at angles of 72° about the central axis. Sections from the other tubes (Fig. 10, *b* and *c*) lack rotational symmetry and all of the molecules in these tubes are therefore cut in different places. The molecule located near the middle of each figure also presents a slightly different section in each case, because the lattices have different orientations with respect to the tube axis.

The density variation inside the tube, where there is only ice and no specimen, indicates the level of noise. In each example, the averaging of 7,000 to 9,000 molecules has, in this

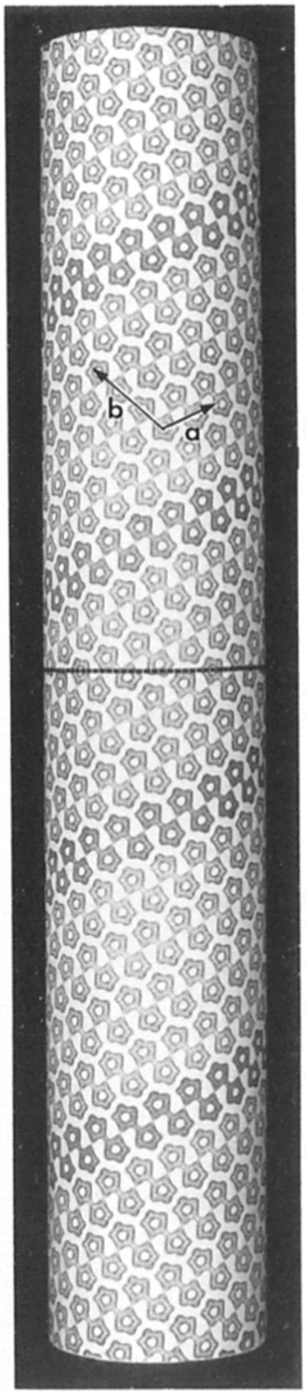

Figure 9. Cylindrical shell calculated for a tube belonging to the (−15, 5) class at a radius of 300 Å (just outside the membrane). One ribbon of paired receptors, which follows the *a* cell vector and gives rise to the (0, *k*; 5*k*) layer-lines, is shaded. Sections at the horizontal line near the middle of the tube are shown in Fig. 10.

region, led to a local density variation of less than two contour levels, or <1/10 of the contrast where the specimen is located. The noise level is higher in Fig. 10 *b* and *c* than in Fig. 10 *a*, reflecting a smaller number of molecules in the average. However, the general features of the receptor and lipid bilayer in each example are the same.

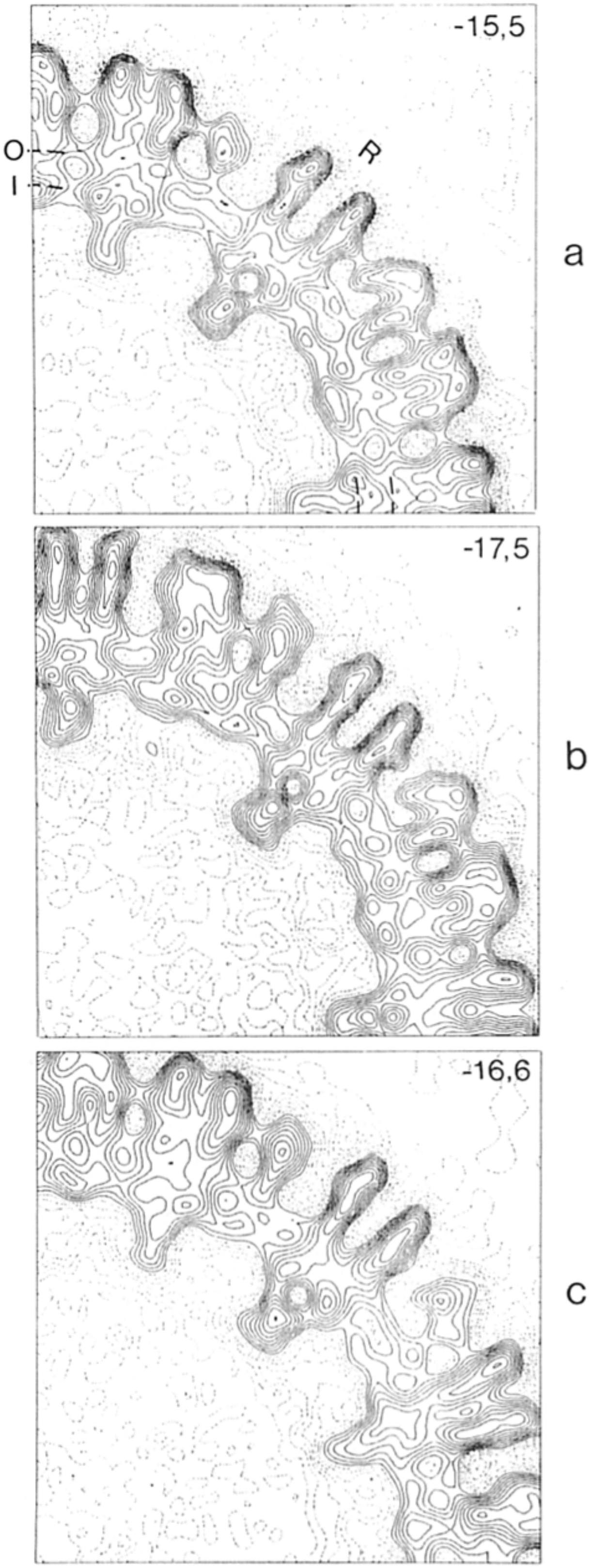

Figure 10. Cross sections of three classes of tubes reconstructed from averaged datasets: *a*, (−15, 5); *b*, (−17, 5); *c*, (−16, 6) classes. These sections correspond to the horizontal line in Fig. 9. Only a quadrant, from a radius of 0–380 Å, is shown. The tube axis is located at the bottom left corner of each panel. Note that receptors are cut at different levels (see Fig. 9); only the one near the middle of each figure (*R* in *a*) shows a section cut through the center of a molecule. Due to the difference in orientation of the unit cells relative to the tube axis, all three show slightly different cross sections of the receptor. Note that the two leaflets of the lipid bilayer (*O* and *I* in *a*) are resolved.

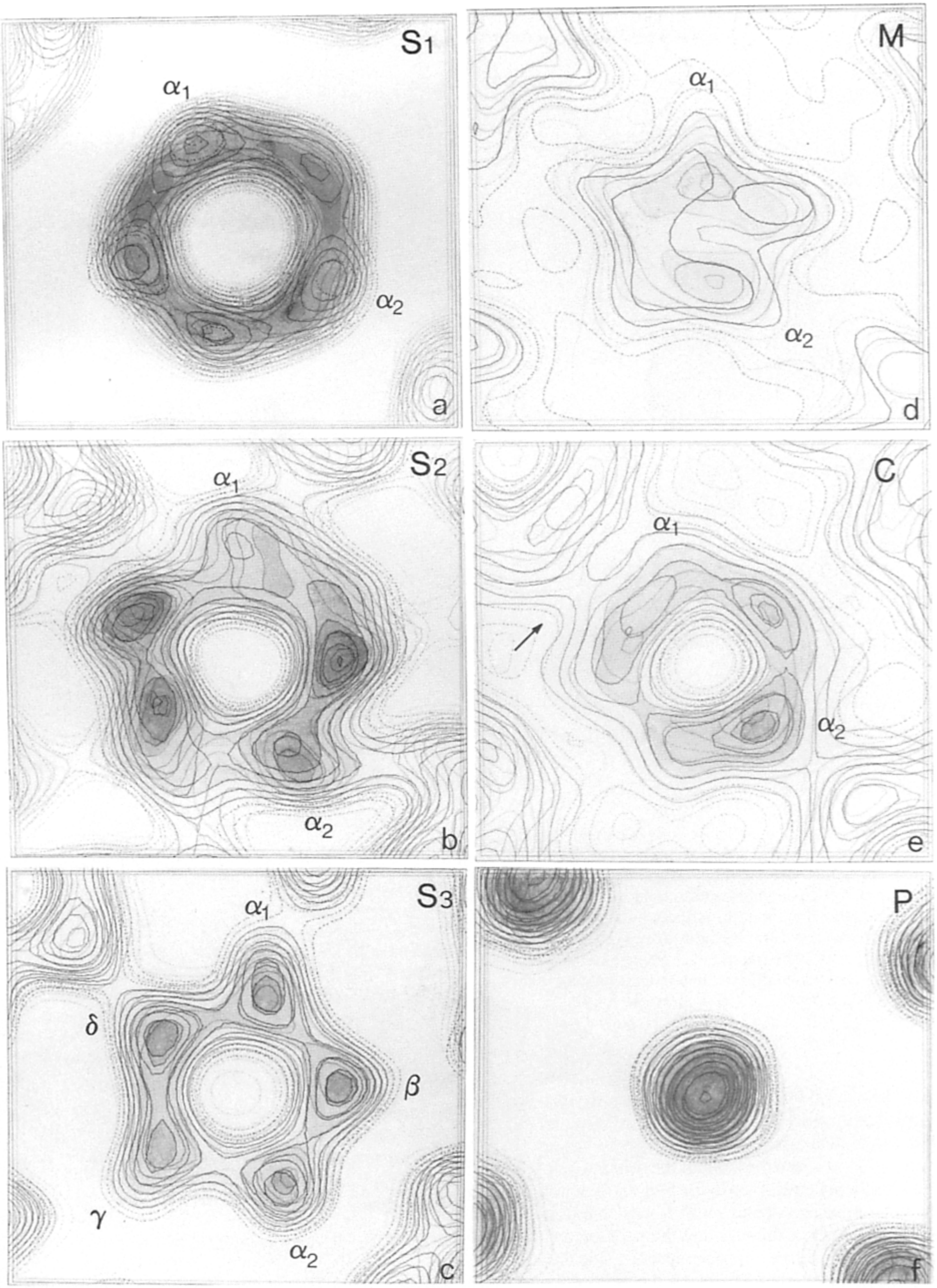

Figure 11. Stacks of vertical sections normal to the radius of the tube, which cut through the receptor in planes normal to the pseudo fivefold axis. From top left to bottom right: the synaptic end of the receptor (*S_1*), middle part on the synaptic side (*S_2*), just above the membrane (*S_3*), middle of the membrane (*M*), cytoplasmic part (*C*), and a peripheral density associated with the receptor (*P*). Each frame consists of a stack of three sections spaced 6 Å apart, except for *S_1* and *P* where four sections are superimposed. Note that the degree of fivefold symmetry varies considerably at different levels. Solid and broken lines enclose respectively ~81 and ~100% of the expected volume of the receptor (consisting of *S_1*, *S_2*, *S_3*, *M*, and *C*) assuming a molecular weight of 285,000 and a specific volume of 0.75 for the glycosylated protein (33). The assignment shown for the α_1, β, α_2, γ, and δ subunits is based on the study of Kubalek et al. (27). One frame covers 110 × 100 Å.

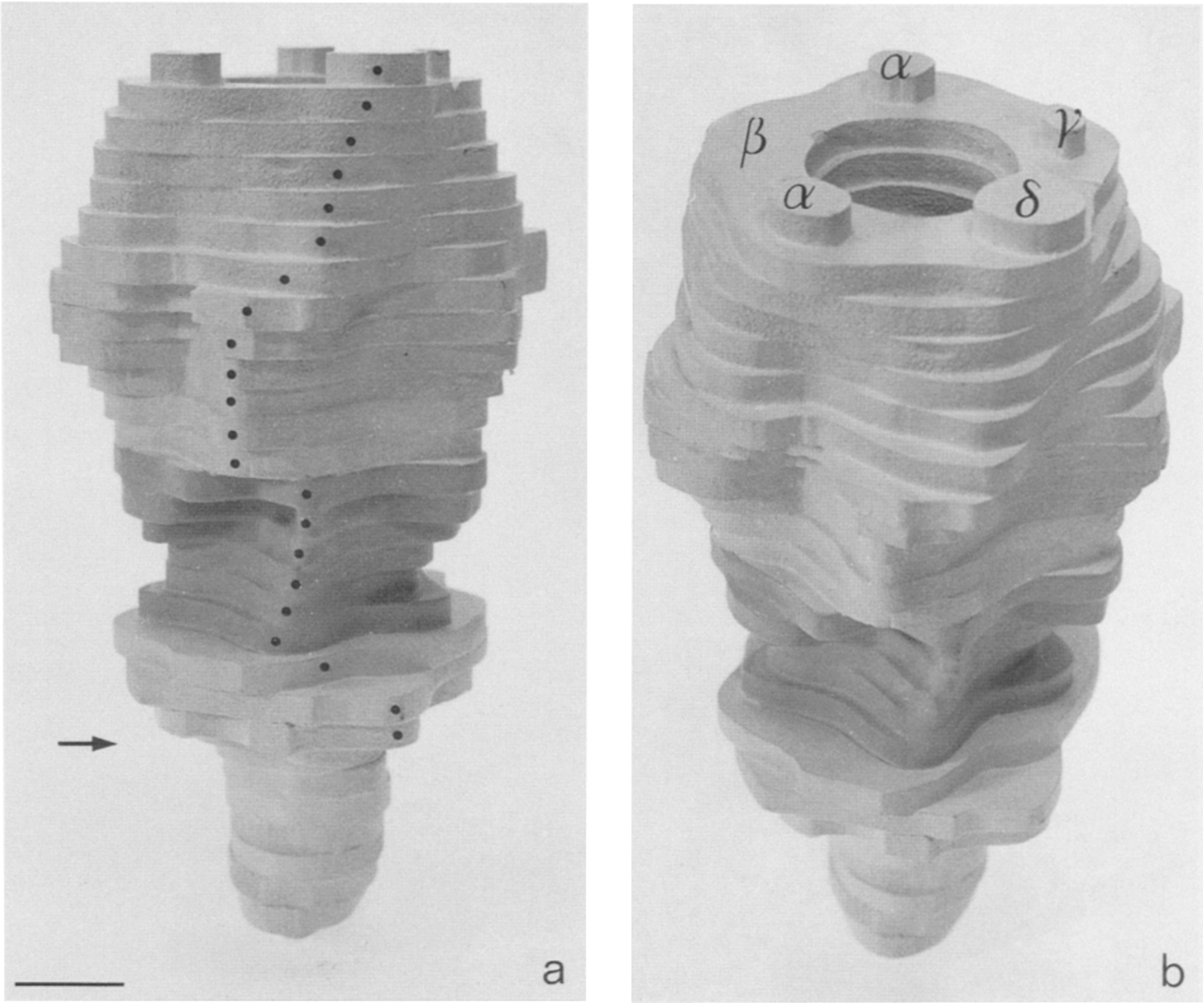

Figure 12. Two (*a*, horizontal and *b*, oblique) views of a wooden model of the acetylcholine receptor. The shaded part indicates the portion contacting the hydrophobic region of the lipid bilayer. The cytoplasmic end of the receptor is thought to be at the level indicated by the arrow in *a*, and the presumed 43K protein is at the bottom (37). To obtain the model one molecule was cut out of the density map by projecting a number of rays from the pseudo-fivefold axis of the receptor and tracing the minimum density points on the rays. Flat faces and sharp edges, conspicuous at about the halfway on the synaptic side, are due to apparent contacts between the neighboring receptors. The oblique view (*b*) shows how abruptly the structure changes at the interface between transmembrane and cytoplasmic parts. The dotted line in *a* follows the ridge of the δ subunit. The volume of the model above the arrow is 283,000 Å^3; this value corresponds to the 81% of the expected volume. At this cut-off level it is assumed that the contribution from lipid to the surface features is negligible. The thickness of each slab is 5.6 Å. Bar, 20 Å.

The profile of the central ion pathway is most clearly seen in these sections. Confirming our earlier findings based on analysis of just one helical family (37), the pathway has an almost constant (~25 Å) width throughout the synaptic portion, but is too narrow to be resolved in the bilayer-spanning region (the diameter presumably being <10 Å). Another feature common to all classes of tubes is that the pathway narrows less abruptly into the bilayer from the synaptic side than from the cytoplasmic side. The density on the axis of the pore is also highest on the cytoplasmic side. Therefore the narrowest portion of the pore is closer to the cytoplasmic opening, and this is where the gate of the ion channel is most likely to be located.

Vertical Sections. Vertical sections (i.e., views normal to the radius of the tube [Fig. 11]) reveal associations between neighboring receptors in the crystal lattice. These were not evident in earlier maps from the flattened tubes, where the resolution perpendicular to the membrane plane was poorer (3, 39). The sections shown in Fig. 11 are derived from the (-15, 5) class; the sections from the other classes appear virtually identical (data not shown).

On the synaptic side, neighboring molecules appear to make contact at two levels: one just above the bilayer (Fig. 11 *c*) and the other about midway between the bilayer at the top of the molecule (Fig. 11 *b*). At the former level, the associations appear to involve both the δ and the α subunits, whereas at the latter level the cross section of the molecule is larger and all the subunits, if not contacting, at least come very close to one another. On the cytoplasmic side, the cross section again becomes larger, and quite extensive connections again appear to be made, but this time only along one direction (Fig. 11 *e*), which corresponds to the *b* direction of the unit cell (Fig. 3). However, the apparent contact becomes weaker and the gap (*arrow*, Fig. 11 *e*) wider as the tube becomes larger (data not shown). Hence interaction at this level is unlikely to be important in generating the lattice but may have a role in setting a lower limit for the diameter of the tubes.

Structure of a Single Molecule

The vertical sections just described show the detailed structure of a single molecule. Wooden models also have been constructed from them to illustrate the overall surface appearance. It is simplest to use both representations together in describing the molecular features. Since the wooden models for the different classes of tubes are very similar to one another, here again, only the model for the (−15, 5) class is shown (Fig. 12).

Taking first the synaptic portion, we observe that the subunits, delineated by ridges on the wooden model (Fig. 12), all end at approximately the same level. The ridges follow curved paths, and twist noticeably near the top of the molecule, in a right-handed sense. The ridges are quite prominent near the membrane but broad and smooth near the synaptic end; surface features are more complicated in the middle region. This varying appearance of the ridges is manifested as three zones of distinct character in vertical cross sections (S_1, S_2, and S_3 in Fig. 11). In the uppermost zone (Fig. 11, S_1) the subunits all look similar, but the fivefold modulations resulting from their pentagonal arrangement is rather weak (except at the very top). In the middle zone (Fig. 11, S_2) the subunits appear bulkier and differ more significantly in individual appearance. Closer to the membrane surface (Fig. 11, S_3) the subunits appear as five straight columns of density and the fivefold symmetry becomes conspicuous.

The structure changes quite dramatically at the level of the phospholipid head groups (Fig. 12). The receptor in the bilayer has a narrower cross section and the ridges made by the subunits, although still prominent, are displaced anticlockwise by ~20°, reflecting probably a change in internal folding of the polypeptide chain.

In the cytoplasmic portion (Fig. 11 *e*), the cross section of the subunits increases, but the fivefold symmetry becomes weaker and the subunit–subunit boundaries become less distinct. The change in structure at the membrane surface is again abrupt. Thus, in the wooden model (Fig. 12 *b*), the narrow highly modulated membrane spanning region (*shaded area*) changes to the broad cytoplasmic region in the next section. Finally, at the bottom of the structure (Fig. 11 *d*) is the central density that shows prominently in the cross-sectional view (Fig. 10) and is thought not to be a part of the receptor itself.

Overall then, the receptor has an elongated structure with features organized pseudo-pentagonally around the ion pathway. The structure can be described in terms of dimensions and volumes, although values are only approximate since disordered parts of the structure are not visualized and the molecular boundaries, at 17 Å resolution, are not precise. The molecule fits within a cylinder of 80 Å diam and 125 Å long. At the cutoff level chosen for constructing the wooden model (see the legend to Fig. 12), the synaptic part (Fig. 11, *S*) occupies ~55% of total volume and is 65 Å long. The transmembrane part occupies ~25% of total volume; the part contacting the hydrophobic region of the lipid bilayer (Fig. 11, *M*) is ~30 Å long and has a cross section of ~1,800 Å² (at 81% volume recovery). The cytoplasmic part (Fig. 11, *C*) occupies ~20% of total volume and is ~20 Å long.

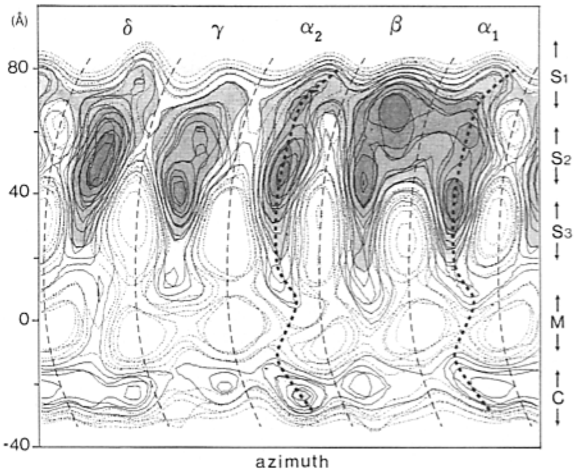

Figure 13. Radial projection of a single receptor, obtained by superimposing cylindrical sections calculated for radii of 27.5, 30, and 32.5 Å around the pseudo-fivefold axis. The view is from the outside toward the pseudo-fivefold axis, with the synaptic end of the receptor at the top. The horizontal axis shows the azimuthal angle around the pseudo-fivefold axis and the vertical axis represents the distance from the center of the lipid bilayer. This contour map describes the density distribution at outer radii of the molecule; the density belonging to the presumed 43K protein is at too small a radius to contribute to the map. Portions covered by the stacks of cross sections (Fig. 11) are indicated at the right hand side. Thin broken lines, separated by 72°, follow roughly the boundaries of the subunits. The paths of the two α subunits are traced by two identical dotted lines. Solid and broken lines correspond to the same levels as in Fig. 11. The sections superimposed were calculated by interpolation from the three-dimensional density array used for generating vertical sections (Fig. 11).

Paths Taken by the Subunits

The difference between the subunits, and their similarities, are most clearly revealed in radial projections about the pseudo fivefold axis. Fig. 13 shows such a radial projection, made by calculating the densities on a series of cylindrical sections at radii between 27.5 and 35 Å, superimposing the sections, and laying them out flat.

First, we note that the densities corresponding to the two α subunits follow the same paths (*dotted lines* in Fig. 13). In both cases, the densities are angled in the same way near the top of the molecule, and their paths are "kinked" in the same way at the membrane surface. Peaks of density on the cytoplasmic side of the membrane are in the same relative positions as well. Differences that are evident (e.g., at the level corresponding to S_2 and S_3) can largely be accounted for by the fact that densities near the surface are affected by the contacts with neighboring molecules, which for the two αs are not equivalent.

The other subunits all show similar general features, e.g., the twisting near the top and the kinking at the membrane. However, the δ subunit is clearly the largest subunit and starts to incline closer to the membrane than the other subunits. The γ appears to be slightly wider than the others at the S_2 and S_3 levels, and the β is more similar to the γ than to the δ or to the α subunits.

Discussion

This paper reports the structure of the nicotinic acetylcholine receptor in *Torpedo* postsynaptic membranes, determined by cryoelectron microscopy and helical image reconstruction. The resolution obtained (17 Å) has been sufficient to resolve the two halves of the lipid bilayer (Fig. 10). We have also shown that the two identical subunits (the αs) are very similar and somewhat different from the other subunits (Fig. 13), as would be expected. Furthermore, reconstructions from images of tubes having different diameters and belonging to different helical families all gave essentially the same structure for the molecule itself. Not all these criteria have been met in earlier studies, and we believe therefore that the structure derived in this analysis provides the most accurate picture yet.

The three-dimensional maps confirmed that the receptor is an elongated molecule, on average ~70 Å in diameter and 125 Å long. In detail, however, it has a partitioned appearance; the structure changing in a similar way for each of the subunits at different levels relative to the membrane. The molecule is widest in the middle of the synaptic portion (~80 Å across) and on the cytoplasmic side (~70 Å across); it is narrowest in the hydrophobic part of the bilayer (~55 Å across). The cross section in the bilayer-spanning portion (~1,800 $Å^2$ at 81% volume recovery) is in good agreement with the proposal that there are only four transmembrane α-helices per subunit (8, 12, 31), assuming packing similar to that in bacteriorhodopsin (~110 $Å^2$ per helix [18]); however, we cannot totally rule out other possibilities (14, 17, 34) since the maps do not give a precise indication of the protein–lipid boundary. The subunits are similar, but show significant individual differences. They are all inclined tangentially near the top of the molecule, producing a twisted configuration, and there is a noticeable displacement of their paths at the membrane surfaces suggesting a change there in the tertiary folding of the polypeptide chains.

The subunits most obviously involved in associations with those of neighboring receptors are the δ and α subunits. δ-δ subunit and α-α subunit contacts seem to be made at a level just above the membrane on the synaptic side, creating a pattern of interactions that may be the same as that responsible for the dimer ribbons found in the native *Torpedo* postsynaptic membranes (19). The δ subunits of neighboring receptors are linked to each other through disulphide bonds (4, 27) and the observed association may reflect this covalent interaction, which is thought to be on the synaptic side (13, 29). A tendency for receptors to associate through their α subunits in the native membranes has been noted in fluorescence energy transfer studies (23).

The ion pathway itself is divided into three regions, with sharp transitions occurring at the level of the phospholipid headgroups. There are two 20–25-Å-wide entrances on either side of the membrane and, between them, a narrow pore that extends just through the hydrophobic part of the bilayer. The dimensions of the pore are too small to be apparent at this resolution; however, the densities on the molecule axis are consistently higher in the cytoplasmic half of the bilayer. Thus, the pore seems to be more constricted on this side, suggesting that the gate may be located here. The length of the narrowest portion might be short (10).

Earlier cryoelectron microscopy studies, using flattened tubes, showed similar features to these (3, 39); however, the resolution was considerably poorer in the direction perpendicular to the membrane, so that much of the fine detail was blurred in this direction. Hence it was not possible to observe the configuration of contacts between neighboring receptors, nor was the shape of the channel well represented. It seems likely that the densities corresponding to the presumed 43K protein merged with those of the receptor and, in effect, filled the cytoplasmic entrance to the channel.

In a recent study of flattened tubes from *Torpedo californica*, Mitra et al., (30) used a dilute staining reagent (0.2% uranyl acetate) and dried and wetted the specimen several times before the stain was applied. It is likely that the stain did not penetrate the tubes properly under these conditions, since the contrast of features on the cytoplasmic side of the membrane was poorer than inside the membrane, where the stain is not expected to produce contrast, and the cytoplasmic opening to the channel was not resolved. Furthermore, the densities in a difference map, attributed to the 43K protein, were close to the noise level, and comparable to density variations in other parts of the structure, e.g., underneath the pore. It is therefore difficult to relate the pattern of stain penetration, found in that study, to features of the protein contrasted against water and lipid as found here.

While the structure of the receptor is not yet sufficiently well resolved to allow any firm deductions to be made, there are several details that seem to reflect the known or deduced properties of the folded polypeptide chains and that correlate with results of physiological experiments. First, the subunits all change their appearance in similar ways, at similar levels relative to the membrane, as might be expected since the tertiary folding of the homologous polypeptides must be largely the same. On the synaptic side, the main regions of individual difference are at ~30 Å above the membrane, and since the subunits have different degrees of glycosylation (9, 32), this may be where most of the sugar is located. Both the δ and the γ subunits, which are extensively glycosylated, are especially bulky at this level. On the cytoplasmic side, the subunits also show significant individual differences, reflecting perhaps the greater departures from homology in this region (5). Second, the observed abrupt change in structure at the level of the phospholipid headgroups is consistent with features of the amino acid sequence. For example, nearly all the synaptic mass is derived from the amino-terminal 1 to 210–224 amino acids (5), and the links on this side between the putative transmembrane α-helices are not extensive, suggesting the synaptic portion is a separate structural domain. Finally, the finding that the most constricted part of the channel is in the cytoplasmic leaflet of the bilayer is in line with the results of combined mutagenesis and physiological experiments (6, 22, 28) showing that residues towards the cytoplasmic end of the putative pore-lining α-helix, M2, have a critical effect on the ion transport behavior.

This research was supported in part by a Muscular Dystrophy Association Postdoctoral Fellowship to C. Toyoshima and by a grant from the National Institutes of Health.

Received for publication 28 June 1990 and in revised form 17 August 1990.

References

1. Amos, L. A., and A. Klug. 1975. Three-dimensional image reconstructions of the contractile tail of T4 bacteriophage. *J. Mol. Biol.* 99:51–73.
2. Brisson, A., and P. N. T. Unwin. 1984. Tubular crystals of acetylcholine receptor. *J. Cell Biol.* 99:1202–1211.
3. Brisson, A., and P. N. T. Unwin. 1985. Quaternary structure of the acetylcholine receptor. *Nature (Lond.).* 315:474–477.
4. Chang, H. W., and E. Bock. 1977. Molecular forms of acetylcholine receptor. Effects of calcium ions and sulfhydryl reagent on the occurrence of oligomers. *Biochemistry.* 16:4513–4520.
5. Changeux, J.-P., A. Devillers-Thiery, and P. Chemouilli. 1984. Acetylcholine receptor: an allosteric protein. *Science (Wash. DC).* 225:1335–1345.
6. Charnet, P., C. Labarca, R. J. Leonard, N. J. Vogelaar, L. Czyzyk, A. Gowin, N. Davidson, and H. A. Lester. 1990. An open-channel blocker interacts with adjacent turns of α-helices in the nicotinic acetylcholine receptor. *Neuron.* 4:87–95.
7. Claudio, T. 1989. Molecular genetics of acetylcholine receptor channels. *In* Frontiers in Molecular Biology. D. M. Glover and B. D. Hames, editors. IRL Press, Oxford, England. 63–142.
8. Claudio, T., M. Ballivet, J. Patrick, and S. Heinemann. 1983. Nucleotide and deduced amino acid sequences of *Torpedo californica* acetylcholine receptor γ subunit. *Proc. Natl. Acad. Sci. USA.* 80:1111–1115.
9. Claudio, T., H. L. Paulson, W. N. Green, A. F. Ross, D. S. Hartman, and D. Hayden. 1989. Fibloblasts transfected with *Torpedo* acetylcholine receptor β-, γ-, and δ-subunit cDNAs express functional receptors when infected with a retroviral α recombinant. *J. Cell Biol.* 108:2277–2290.
10. Dani, J. A. 1989. Open channel structure and ion binding site of the nicotinic acetylcholine receptor channel. *J. Neurosci.* 9:884–892.
11. DeRosier, D. J., and P. B. Moore. 1970. Reconstruction of three-dimensional images from electron micrographs of structures with helical symmetry. *J. Mol. Biol.* 52:355–369.
12. Devillers-Theiry, A., J. Giraudat, M. Beutaboulet, and J.-P. Changeux. 1983. Complete mRNA coding sequence of the acetylcholine binding α subunit of *Torpedo marmorata* acetylcholine receptor: a model for the transmembrane organization of the polypeptide chain. *Proc. Natl. Acad. Sci. USA.* 80:2067–2071.
13. DiPaola, M., C. Czajkowski, and A. Karlin. 1989. The sidedness of the COOH terminus of the acetylcholine receptor δ-subunit. *J. Biol. Chem.* 264:15457–15463.
14. Finer-Moore, J., and R. M. Stroud. 1984. Amphipathic analysis and possible formation of the ion channel in an acetylcholine receptor. *Proc. Natl. Acad. Sci. USA.* 81:155–159.
15. Giraudat, J., M. Dennis, T. Heidemann, J.-Y. Chang, and J.-P. Changeux. 1986. Structure of the high-affinity binding site for non-competitive blockers of the acetylcholine receptor: serine-262 of the δ-subunit is labeled by [^{3}H]chlorpromazine. *Proc. Natl. Acad. Sci. USA.* 83:2719–2723.
16. Giraudat, J., M. Dennis, T. Heidemann, P.-Y. Haumont, F. Lederer, and J.-P. Changeux. 1987. Structure of the high affinity binding site for noncompetitive blockers of the acetylcholine receptor: [^{3}H]chlorpromazine labels homologous residues in the β and δ chains. *Biochemistry.* 26:2410–2418.
17. Guy, H. R. 1984. Structural model of the acetylcholine receptor channel based on partition energy and helix packing considerations. *Biophys. J.* 45:249–261.
18. Henderson, R., and P. N. T. Unwin. 1975. Three-dimensional model of purple membrane obtained by electron microscopy. *Nature (Lond.).* 257:28–32.
19. Heuser, J. E., and S. R. Salpeter. 1979. Organization of acetylcholine receptors in quick frozen, deep etched, and rotary-replicated *Torpedo* postsynaptic membrane. *J. Cell Biol.* 82:150–173.
20. Hille, B. 1984. Ionic Channels of Excitable Membranes. Sinauer Associates, Inc., Sunderland, MA. 1–426.
21. Hucho, F., W. Oberthür, and F. Lottspeich. 1986. The ion channel and the nicotinic acetylcholine receptor is formed by the homologous helices MII of the receptor subunits. *FEBS (Fed. Eur. Biochem. Soc.) Lett.* 205:137–142.
22. Imoto, K., C. Busch, B. Sakmann, M. Mishina, T. Konno, J. Nakai, H. Bujo, Y. Mori, K. Fukuda, and S. Numa. 1988. Rings of negatively charged amino acids determine the acetylcholine receptor channel conductance. *Nature (Lond.).* 335:645–648.
23. Johnson, D. A., J. G. Voet, and P. Taylor. 1984. Fluorescence energy transfer between cobra α-toxin and molecules bound to the acetylcholine receptor. *J. Biol. Chem.* 259:5715–5725.
24. Karlin, A., P. N. Kao, and M. Di Paola. 1986. Molecular pharmacology of the nicotinic acetylcholine receptor. *Trends Pharmacol. Sci.* 7:304–308.
25. Kistler, J., and R. M. Stroud. 1981. Crystalline arrays of membrane-bound acetylcholine receptor. *Proc. Natl. Acad. Sci. USA.* 78:3678–3682.
26. Klug, A., F. H. C. Crick, and H. W. Wykoff. 1958. Diffraction by helical structures. *Acta Cryst.* 11:199–213.
27. Kubalek, E., S. Ralston, J. Lindstrom, and N. Unwin. 1987. Location of subunits within the acetylcholine receptor by electron image analysis of tubular crystals from *Torpedo marmorata. J. Cell Biol.* 105:9–18.
28. Leonard, R. J., C. G. Labarca, P. Charnet, N. Davidson, and H. A. Lester. 1988. Evidence that the M2 membrane-spanning region lines the ion channel pore of the nicotinic receptor. *Science (Wash. DC).* 242:1578–1581.
29. McCrea, P. D., J.-L. Popot, and D. M. Engelman. 1987. Transmembrane topography of the nicotinic acetylcholine receptor δ submit. *EMBO (Eur. Mol. Biol. Organ.) J.* 6:3619–3626.
30. Mitra, A. K., M. P. McCarthy, and R. M. Stroud. 1989. Three-dimensional structure of the nicotinic acetylcholine receptor and location of the major associated 43-kD cytoskeletal protein, determined at 22 Å by low dose electron microscopy and x-ray diffraction to 12.5 Å. *J. Cell Biol.* 109:755–774.
31. Noda, M. H., T. Takahashi, M. Tanabe, S. Toyosato, Y. Kikyotani, T. Furutani, H. Hirose, H. Takashima, S. Inayama, T. Miyata, and S. Numa. 1983. Structural homology of *Torpedo californica* acetylcholine receptor subunits. *Nature (Lond.).* 302:528–532.
32. Nomoto, J., N. Takehashi, Y. Nagaki, S. Endo, Y. Arata, and K. Hayashi. 1986. Carbohydrate structures of acetylcholine receptor from *Torpedo californica* and distribution of oligosaccharide among the subunits. *Eur. J. Biochem.* 157:233–242.
33. Popot, J.-L., and J.-P. Changeux. 1984. The nicotinic receptor of acetylcholine: structure of an oligomeric integral membrane protein. *Physiol. Rev.* 64:1162–1239.
34. Ratnam, M., D. Le Nguyen, J. Rivier, P. B. Sargent, and J. Lindstrom. 1986. Transmembrane topography of nicotinic acetylcholine receptor: immunochemical tests contradict theoretical predictions based on hydropathy profiles. *Biochemistry.* 25:2633–2643.
35. Revah, F., J.-L. Galzi, J. Giraudat, P.-Y. Haumont, F. Lederer, and J.-P. Changeux. 1990. The noncompetitive blocker [^{3}H]chlorpromazine labels three amino acids of the acetylcholine receptor γ-subunit; implications for the α-helical organization of the MII segments and the structure of the ion channel. *Proc. Natl. Acad. Sci. USA.* 87:4675–4679.
36. Toyoshima, C. 1989. On the use of holey grids in electron crystallography. *Ultramicroscopy.* 30:439–444.
37. Toyoshima, C., and N. Unwin. 1988. Ion channel of acetylcholine receptor reconstructed from images of postsynaptic membranes. *Nature (Lond.).* 336:247–250.
38. Toyoshima, C., and N. Unwin. 1988. Contrast transfer for frozen-hydrated specimens: determination from pairs of defocused images. *Ultramicroscopy.* 25:279–292.
39. Unwin, N., C. Toyoshima, and E. Kubalek. 1988. Arrangement of the acetylcholine receptor subunits in the resting and desensitized states, determined by cryoelectron microscopy of crystallized *Torpedo* postsynaptic membranes. *J. Cell Biol.* 107:1123–1138.
40. Wakabayashi, T., H. E. Huxley, L. A. Amos, and A. Klug. 1975. Three-dimensional image reconstruction of actin-tropomyosin complex and actin-tropomyosin-troponin T-troponin I complex. *J. Mol. Biol.* 93:477–497.